IAC-20-A6.5.5

Simulation and Laboratory Testing of the 3U CubeSat Control in the Proximity of Space Debris

Danil Ivanov[a]*, Michael Ovchinikov[b], Mahdi Akhloumadi[c], Filipp Kozin[d], Per-Erik Atterwall[e]

[a] Space Systems Dynamics Department, Keldysh Institute of Applied Mathematics, RAS, Moscow, Russian Federation danilivanovs@gmail.com
[b] Space Systems Dynamics Department, Keldysh Institute of Applied Mathematics, RAS, Moscow, Russian Federation, ovchinni@keldysh.ru
[c] Moscow Institute of Physics and Technology, Moscow Region, Russia, akhloumadi@gmail.com
[d] Space Systems Dynamics Department, Keldysh Institute of Applied Mathematics, RAS, Moscow, Russian Federation filipp.kozin@gmail.com
[e] Beyond Atlas, Sweden, per-erik@attwik.se

* Corresponding Author

Abstract

The goal of the proposed 3U CubeSat mission is to test GNC system for a future flight to a near Earth asteroid. In order to gain the goal a 3U CubeSat is to get to a vicinity of a space debris in a sun-synchronous LEO. In the paper a scheme of the safe autonomous controlled relative motion of the CubeSat in the predefined relative area is proposed. An extended Kalman filter onboard the CubeSat is used to estimate the relative state vector. Using this vector and the covariance error matrix, the relative trajectory is predicted by integrating the equations of relative motion over the next two hours of flight. When the satellite position error ellipsoid reaches a dangerous distance with respect to the space debris, a collision avoidance maneuver is applied to achieve a safe relative distance. To provide necessary stabilization to the debris direction for the laser range finder measurements it is necessary to obtain optical sensor measurements available only for the illuminated part of the orbit. In case when the measurements are not available the current state vector is estimated using only the integration of the motion equations. The proposed scheme of the controlled motion is tested in the laboratory facility COSMOS at KIAM using air bearing planar test bed. A debris mock-up and the 3U CubeSat mock-up equipped with thruster imitators move almost frictionless along the surface, and thus the relative motion in the orbital plane is simulated. The results of the control algorithm tests are presented in the paper.

Keywords: Space debris removal, collision avoidance, laboratory testing, aerodynamic testbed

1. Introduction

Currently, there are different approaches to solving the problem of space debris. One of the ways is to launch special small spacecraft that are able to attach to a non-cooperative object and, using a propulsion system, change the orbit of space debris. With such a debris removal scheme, the task of controlling the relative motion of the spacecraft during the approach to an arbitrarily rotating object arises. To increase the probability of mission success, the developed control algorithms are tested in ground conditions using special laboratory stands.

The active space debris removal using small satellite can be divided at several stages. First, the space debris should be observed from safe relative distance in order to determine its angular motion and possible point for the capturing. For this stage the natural closed relative trajectory should be obtained by the active satellite control system. However, due to disturbances the relative drift can appear. In that case if the relative distance between the satellite and the debris become dangerous a collision avoidance maneuver should be applied, moreover after its execution the relative distance should remain suitable for the debris observation. The paper proposes a set of rendezvoius control algorithms applications from the far range and a controlled motion scheme in the debris observation stage of the proposed mission.

2. 3U CubeSat details

The goal of the proposed 3U CubeSat mission is to test GNC system for a future flight to a near Earth asteroid. In order to gain the goal a 3U CubeSat is to get to a vicinity of a space debris in a sun-synchronous LEO. The CAD model of the 3U Cube Sat presented in Fig. 1. The satellite GNC system includes on-board propulsion, magnetorquers, reaction wheels and attitude determination sensors. Laser range finder and optical sensor measurements are used for the relative navigation. It is assumed that the maneuver commands to the CubeSat to approach to a vicinity of debris are uploaded from the ground control centre. However, when the distance becomes less than 1 km the

disturbances caused by J2, atmospheric drag and manoeuvre execution errors can lead to dangerous proximity and even to collision with debris during the time interval between the two communication sessions. To provide necessary stabilization to the debris direction for the laser range finder measurements it is necessary to obtain optical sensor measurements available only for the illuminated part of the orbit.

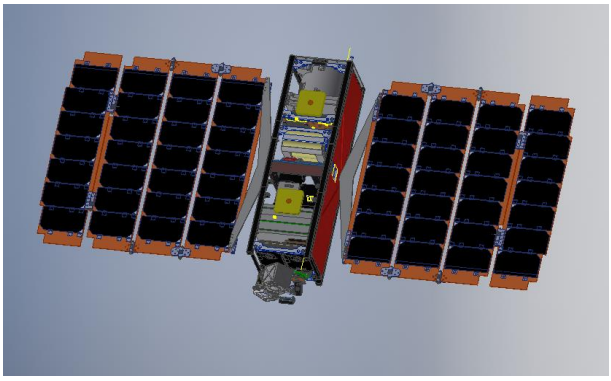

Fig. 1. 3D CAD model of 3U spacecraft

2. Far-range rendezvous strategies

Space rendezvous with respect to mission design can be accomplished by means of different proximity strategies. Here some different optimal approaches to rendezvous trajectory design are discussed, more over the weakness and advantages of each method is studied.

The debris and spacecraft are in orbits with different inclination and semi major axis. The constant electric thruster of the spacecraft liquidate desired impulsive manoeuvres. Here the question rises about superiority of low and constant thrust rendezvous strategies.

The orbital manoeuvre is prior to rendezvous. There are different kinds of orbital manoeuvres such as impulsive and low thrust manoeuvres. In this scheme the aim is to study some different algorithm for optimal proximity manoeuvres [1]. Has done a worthy study on impulsive orbital trajectories. Alongside him in literature, [2] introduced some methods for low-constant thrust proximity manoeuvres using equinoctial orbital elements. Here some of the most common approaches to rendezvous problem is discussed.

.

3.1 Control based on State dependant Riccati equation

SDRE method is a nonlinear suboptimal control approach to obtain the minimizing solution of the quadratic regulator cost function [3]. By solving the algebraic Riccati equation which is state dependant in each time step the optimal control will be gained. In this method the dynamical system must be factorized. This method is studied by authors in space rendezvous and docking [4], [5]. For rendezvous phase the nonlinear form of relative translational equations of motion represented in [4] will be used.

The nonlinear dynamical factorized system has the following form:

$$\begin{aligned} \dot{\mathbf{x}} &= \mathbf{A}\mathbf{x} + \mathbf{B}\mathbf{u} \\ \mathbf{x}(0) &= \mathbf{x}_0 \\ \mathbf{A}(\mathbf{x}(0)) &= 0 \end{aligned} \tag{1}$$

And the quadratic performance measure of:

$$J = \frac{1}{2}\int_0^{t_f} \left[\mathbf{x}(t)^T \mathbf{Q}\, \mathbf{x}(t) + \mathbf{u}(t)^T \mathbf{R}\, \mathbf{u}(t) \right] dt \tag{2}$$

The resulted Riccati equation is given by:

$$\begin{aligned} &\mathbf{P}(\mathbf{x})\mathbf{A}(\mathbf{x}) + \mathbf{A}^T(\mathbf{x})\mathbf{P}(\mathbf{x}) \\ &-\mathbf{P}(\mathbf{x})\mathbf{B}(\mathbf{x})\mathbf{R}^{-1}(\mathbf{x})\mathbf{B}^T(\mathbf{x})\mathbf{P}(\mathbf{x}) + \mathbf{Q}(\mathbf{x}) = 0 \end{aligned} \tag{3}$$

And the optimal control will be:

$$\mathbf{u}(\mathbf{x}) = \mathbf{R}^{-1}\mathbf{B}^T(\mathbf{x})\mathbf{P}(\mathbf{x})\mathbf{x} \tag{4}$$

It is shown that the optimal coefficients **P** can be achieved solving algebraic Riccati equation. Choosing a quadratic cost function in this from containing tracking term and fuel term is logical. However as the thrusters are electrical the second term does not play an important role and the weighting matrix **R** can be chosen as little as possible or can be nullified completely. In SDRE case control constraint are applied to the algorithm as well. Here SDRE algorithm produce the optimal coefficients and produce optimal control then this optimal control is normalized and multiplied by the thruster amplitude to satisfy the low-constant thrust value of controller. The problem formulated as follows:

$$\begin{aligned} J &= \frac{1}{2}\int \mathbf{x}^T\mathbf{Q}\mathbf{x} + \mathbf{u}^T\mathbf{R}\mathbf{u} \\ \mathbf{x}_0 &= \text{specified} \\ \mathbf{x}(tf) &= \text{fixed} \\ t_f &: \text{unspecified} \\ |\mathbf{u}| &: \text{low} - \text{constant}. \end{aligned} \tag{5}$$

3.2 Thrust as orbital perturbation

The other way to accomplish proximity is to consider low thrust as a perturbation to motion and by changing the direction of the constant thrust the desired orbit will be achieved which is studied in [6] [7] [8] .In this case, the Gauss orbital equations for orbital elements can be used:

$$\begin{aligned} \frac{da}{dt} &= \frac{2}{n\sqrt{1-e^2}}\left\{ e\sin(\theta)F_r + \left[1 + e\cos(\theta)\right]F_s \right\} \\ \frac{de}{dt} &= \frac{\sqrt{(1-e^2)}}{na}\left\{ \sin(\theta)F_r + \left[\cos(\psi) + \cos(\theta)\right]F_s \right\} \\ \frac{di}{dt} &= \frac{2}{n\sqrt{1-e^2}}\frac{r}{a}\cos(\theta+\omega)F_w \end{aligned} \tag{6}$$

$$\frac{d\Omega}{dt}=\frac{2}{na\sqrt{1-e^2}}\frac{r}{a}\frac{\sin(\theta+\omega)}{\sin(i)}$$

$$\frac{d\omega}{dt}=\frac{\sqrt{(1-e^2)}}{nae}\left\{-F_r\cos(\theta)+\left[1+\frac{1}{1+e\cos(\theta)}\right]\sin(\theta)F_s-\frac{d\Omega}{dt}\cos(i)\right\}$$

$$\frac{dM}{dt}=n+\frac{1-e^2}{nae}\left\{\left[\frac{-2e}{1+e\cos(\theta)}+\cos(\theta)\right]F_r-\left[1+\frac{1}{1+e\cos(\theta)}\right]\sin(\theta)F_s\right\}.$$

And the directions of thrust are shown as:

$$\begin{aligned}F_r&=|\mathbf{u}|\cos\beta\sin\alpha\\F_s&=|\mathbf{u}|\cos\beta\cos\alpha\\F_W&=|\mathbf{u}|\sin\beta.\end{aligned}\tag{7}$$

The angles α,β and orbital elements are shown in Fig. 2:

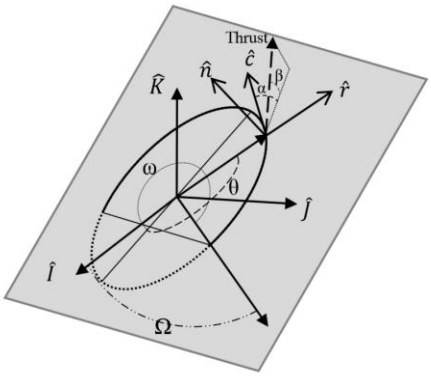

Fig. 2. Orbital elements, Inertial reference frame ($\hat{I}\hat{J}\hat{K}$), body-fixed radial-circumferential-normal ($\hat{r}\hat{n}\hat{c}$) and angles α,β

By taking derivatives with respect to thrust angles α,β, the maximum changes of orbital elements rates will be found. Here the strategy is to compensate inclination and semi-major axis in a sequence to reach the target orbit. With this method it's impossible to achieve the target true anomaly in a planar motion. But it can be shown that with a high accuracy semi major axis and inclination can be changed separately without a considerable change in other orbital elements. From the first and the third of (6) can find out:

$$\alpha=\arctan\left(\frac{e\sin\theta}{1+e\cos\theta}\right),\beta=0\tag{8}$$

For maximum rate of semi major axis, and:

$$\beta=sign(\cos(\omega+\theta)).\frac{\pi}{2},\ \alpha=0\tag{9}$$

Stands for inclination change which shows a normal to orbit thrust direction. The above-mentioned problem is summarized to:

$$\begin{aligned}&J=t_f\\&\mathbf{x}_0=\quad\text{specified}\\&\mathbf{x}(tf)=\text{orbit}\\&t_f:\quad\text{unspecified}\\&|\mathbf{u}|:\quad\text{low}-\text{constant}\end{aligned}\tag{10}$$

3.3 Minimum principle

A third approach is to solve the optimal control problem as a boundary value problem using maximum principle of Pontryagin. The minimum time coast function and the linear appearance of controls in Hamiltonian will lead to a bang-bang control [9]. Here the minimum fuel problem is considered and the minimum time will be addressed using dynamic programming. The similar minimum fuel with bounded control is solved in [10]. Considering performance measure and problem formulation of the form:

$$\begin{aligned}&J=\frac{1}{2}\int\mathbf{u}^{\mathbf{T}}\mathbf{R}\mathbf{u}\\&\mathbf{x}_0=\quad\text{specified}\\&\mathbf{x}(tf)=\quad\text{fixed}\\&t_f:\quad\text{unspecified}\\&|\mathbf{u}|:\quad\text{unbounded},\end{aligned}\tag{11}$$

Recalling that here can take A ((1)) as a linearized form for simplicity which is addressed as Clohessy-Whiltshire equations:

$$A=\begin{bmatrix}0_{3\times3}&1_{3\times3}\\3\omega_o^2&0&0&0&2\omega_o&0\\0&0&0&-2\omega_o&0&0\\0&0&-\omega_o^2&0&0&0\end{bmatrix}.\tag{12}$$

For this system Hamiltonian is:

$$\begin{aligned}H&=p_1x_4+p_2x_5+p_3x_6\\&+3p_4x_1\omega_o^2+2\omega_o p_4x_5-2\omega_o p_5x_4\\&-\omega_o^2p_6x_3+\frac{1}{2}\mathbf{u}^T\mathbf{R}\mathbf{u}+\frac{p_4u_1}{m}+\frac{p_5u_2}{m}+\frac{p_6u_3}{m}.\end{aligned}\tag{13}$$

Using conditions for optimality and(13):

$$\left.\frac{\partial H}{\partial\mathbf{u}}\right|_{\mathbf{u}=\mathbf{u}^*}=0\tag{14}$$

Leads to optimal controls as follow:

$$u_1^* = \frac{-p_4}{2R_1 m_1}$$
$$u_1^* = \frac{-p_5}{2R_2 m_1} \quad (15)$$
$$u_1^* = \frac{-p_6}{2R_3 m_1}.$$

Having Hamiltonian (13) the co-states are as follow:

$$\dot{p}_1 = -\frac{\partial H}{\partial x_1} = -3p_4\omega_o{}^2$$
$$\dot{p}_2 = -\frac{\partial H}{\partial x_2} = 0$$
$$\dot{p}_3 = -\frac{\partial H}{\partial x_3} = p_6\omega_o{}^2 \quad (16)$$
$$\dot{p}_4 = -\frac{\partial H}{\partial x_4} = -p_1 + 2p_5\omega_0$$
$$\dot{p}_5 = -\frac{\partial H}{\partial x_5} = -p_2 - 2p_4\omega_o$$
$$\dot{p}_6 = -\frac{\partial H}{\partial x_6} = -p_3.$$

(12) and (16) are a set of 12 ODE. The problem will be solved having 12 boundary conditions for states and one additional for a co-state as a result of unknown final time. The unconstraint form of problem can be solved for the boundary values and corresponding co-state boundary condition [9].

3.4 Nonlinear programming (NLP)

Here some direct methods are used to solve the optimal control problem using NLP.by direct it means that first the system is discretised and then the optimal solution is approximated or found. we are going to mention two effective way of solving this problem using TOMLAB [11] and JModelica [12] [13], [14]. TOMLAB is a commercial program can be used to solve optimal control problems in MATLAB. TOMLAB supports optimal control in PROPT [15]. PROPT uses a pseudo spectral Collocation method for optimization. JModelica is an open source environment uses allocation method to solve optimal control problem.

Both solvers need initial and final conditions. Moreover an initial guess is to be provided. Both JModelica and TOMLAB are initialized with linear box constraint on controls. In these expression of dynamics the module of control vector is constant. Consequently to initialize solvers with proper control constraint a transformation must be performed. Each moment of time the control vector is:

$$u_x^2 + u_y^2 + u_z^2 = cte. \quad (17)$$

The equation (17) shows a geometrical constraint which represent a sphere. The accessible controls are on the surface of this sphere. In this case a spherical coordinate transformation gives two independent angles θ, φ . These two angles are used to form solvers box constraints. In real case these angles must be expressed with respect to body frame, which can be achieved using a transformation between body frame and LVLH. Finally the time optimal constraint problem has the following form:

$$J = t_f$$
$$\mathbf{x}_0 = \text{specified}$$
$$\mathbf{x}(tf) = \text{fixed} \quad (18)$$
$$t_f : \text{unspecified}$$
$$|\mathbf{u}| : \text{low-constant}$$

4. Results of application of manoeuvre algorithms

In this part the simulation results are presented. The spacecraft located in an orbit which its semi major axis has 5km deviation from semi major axis of the target's orbit. The difference between inclinations of orbits is 5 deg. The spacecraft translational motion is controlled using electrical thrusters limited to 0.00035 N. the specific impulse is 4000s and the satellite weight is assumed to be 3 kg.

The different scenarios are modelled and compared. Considering the simulations has different performance measures and the approach to solve them. First SDRE for quadratic cost function is solved with constraint controls. After that the perturbation constant low thrust is modelled. The SDRE will lead to the following infinity shape relative path. This closed-shape orbit is a well-known formation relative orbit. SDRE control gradually makes it small to the rendezvous point or any specified distance from the target

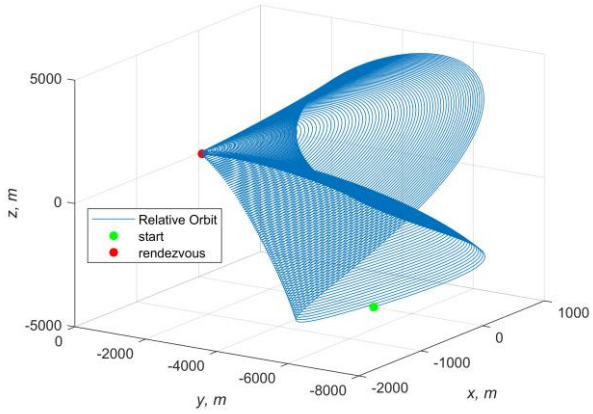

Fig. 3. Relative trajectory using SDRE

Next the inclination and semi-major axis changes are simulated. The two corresponding perturbation

Gaussian equations for a, i with optimal control are shown in Fig. 4. As mentioned the changes of other orbital elements are neglectable. Fig. 5 shows the corresponding thrust angles with respect to body-fixed radial circumferential-normal. Compensation of inclination and semi major axis are separately and uncoupled.

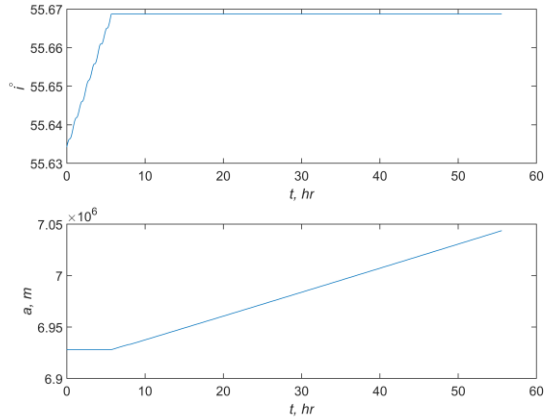

Fig. 4. Inclination and semi major axis change using Gaussian perturbed equation

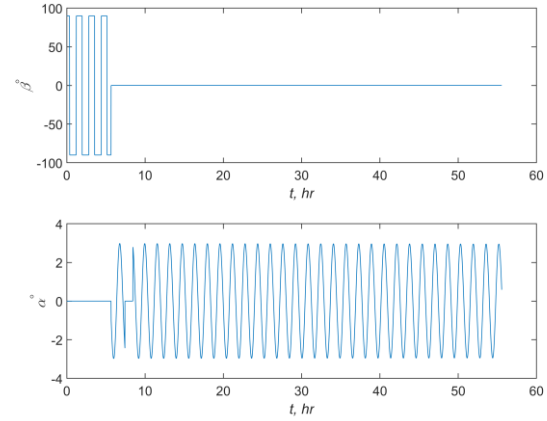

Fig. 5. Control angles of thruster using Gaussian perturbed equation

The trajectory of the minimum fuel problem using minimum principle is shown in Fig. 6. At the beginning the relative distance increases and then it decreases. Fig.7 shows the unbounded low thrust to achieve such a spiral-conic relative orbit.

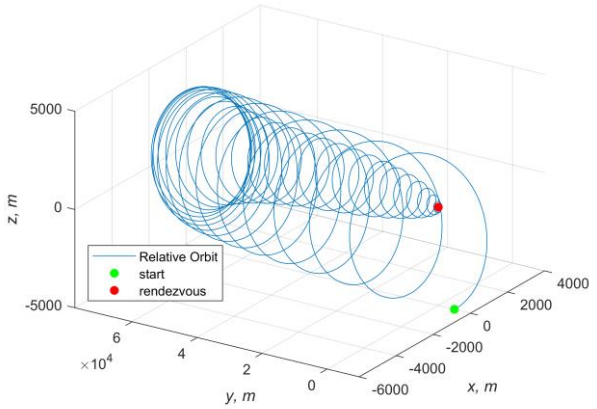

Fig. 6 Relative trajectory of BVP using optimal principle

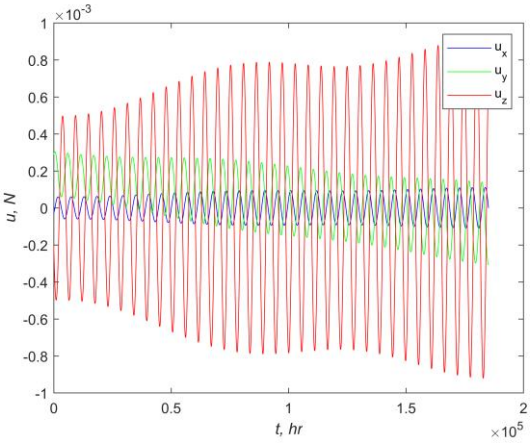

Fig. 7. Controls of BVP using optimal principle

Here the simulations which are conducted by TOMLAB and JModelica are displayed in Fig.8-11. 8 shows the 3D relative trajectory to target in TOMLAB and Fig. 9 express the thrust angles in local spherical coordinate system attached to LVLH. The analogous results in JModelica in Python 2.7 are displayed in Fig. 10 and Fig.11.

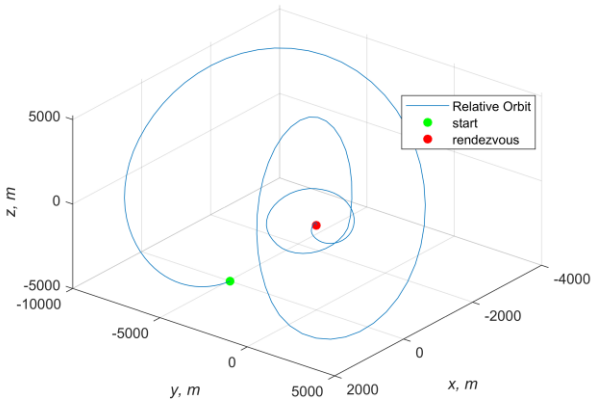

Fig. 8. Relative trajectory using PROPT in TOMLAB environment

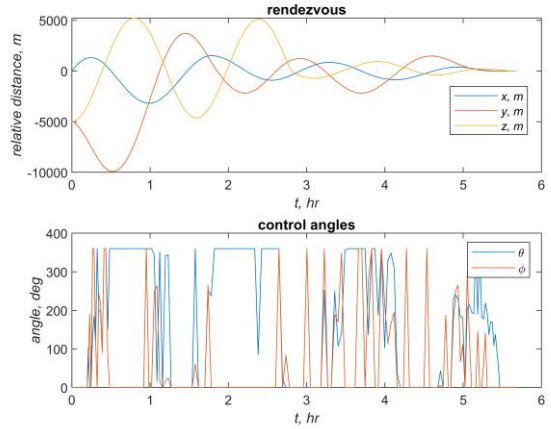

Fig. 9. Relative positions and control angles using PROPT in TOMLAB environment

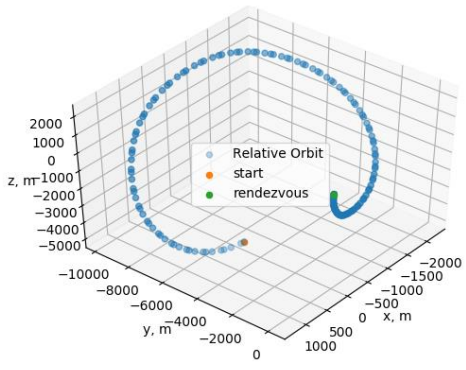

Fig. 10. Relative trajectory using JModelica

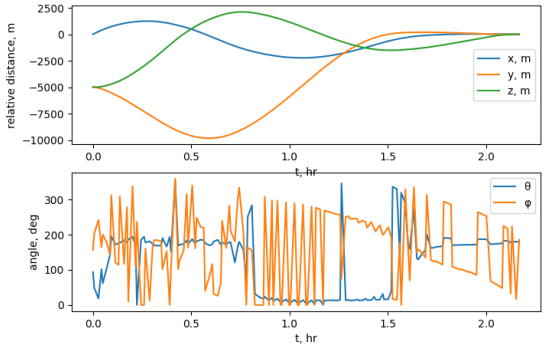

Fig. 11. Relative positions and control angles using JModelica

By using Table 1 it's easy to compare the effectiveness of the studied algorithms and chose the suitable with respect to mission design and requirements. As electrical thrusters are used the fuel consumption is not of a great importance. The rendezvous time can be compromised as well. The run time and required memory play an important role in choosing the proper strategy and solving method. JModelica shows more applicable for real time missions to solve the exact minimum – time problem with less required computational resources.

Table 1. Comparison of different rendezvous strategy and methods

	Problem kind	Run time, s	Memory, MB	time, hr	Fuel consumption, kg
SDRE	NQR-constrained	135	4	5.5	3.7e-3
Minimum principle	Min-fuel-unconstrained	78	149	1.7	2.4e-3
Thrust as perturbation	Min-time-constrained	2	9	56	2.1e-3
TOMLAB	Min-time-constrained	194	242	5.8	2.3e-4
JModelica	Min-time-constrained	21	201	2.3	3.1e-5

5. Laboratory facility description

Laboratory facility COSMOS (COmplex for Satellites MOtion Simulation) consists of the microsatellites mock-ups (Fig 12) placed on the air-bearing table, industrial fan and its control unit, and air supply system (Fig 13) [16–18]. The air bearing table includes the flat perforated aluminum surface and special cavity underneath where the air builds up. The surface of the table consists of two one-cm thick plates. The plates are fixed by a special frame that prevents bending due to the weight of the plates and excessive

pressure. The resulting surface unevenness is about 3.5 mm. The total surface area is 198 by 148 cm. The surface has the pattern of 1 mm diameter holes with 20 mm intervals. The distance between the holes is chosen to provide almost frictionless motion for 30 cm diameter mock-up of up to 6 kg mass. The mock-ups have the shape of an octagonal prism of 40 cm height. Each side has mounting holes that allow hardware installation both inside and outside.

The mock-ups are based on the Orbicraft and Orbicraft-pro construction kit developed by SputniX Ltd [19]. The mass of the bigger mock-up is about 5.2 kg, the axial moment of inertia is about 0.05 $\mathrm{kg}\cdot\mathrm{m}^2$, the mass of the CubeSat-based is about 1.1 kg, the axial moment of inertia is about 0.01 $\mathrm{kg}\cdot\mathrm{m}^2$. Control system imitator includes:

- on-board computer Raspberry PI 2 B;
- power supply system (battery and power management unit);
- set of sensors: magnetometer, Sun sensors, angular velocity sensor, accelerometer;
- set of actuators: reaction wheel, four propellers for the thruster imitation;
- data exchange system;
- on-board camera;
- Wi-Fi module.

There is a special mark on top of each mock-up. The position and attitude of the mock-up is determined using external video camera data processing. This information is transmitted via Wi-Fi channel to the on-board computer. It is then used to generate a control command. In case of autonomous attitude and position determination, the video camera is used as an independent external motion determination system.

The test-bench disturbances were estimated experimentally. Preliminary experiments showed that the air flow from the holes is stationary, i.e. does not vary with time, but rather depends on the location on the table surface. Disturbances acting at some point of the table are almost stationary. So a map of forces and torques acting on the mock-up on the surface of the table may be constructed. This map was constructed by processing the information of the free motion of the mock-up. External video state determination system was used. Linear and angular accelerations of the mock-up were estimated.

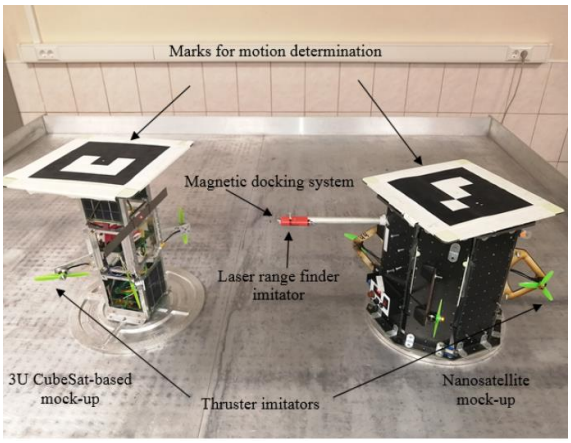

Fig.12. Nanosatellite mock-ups

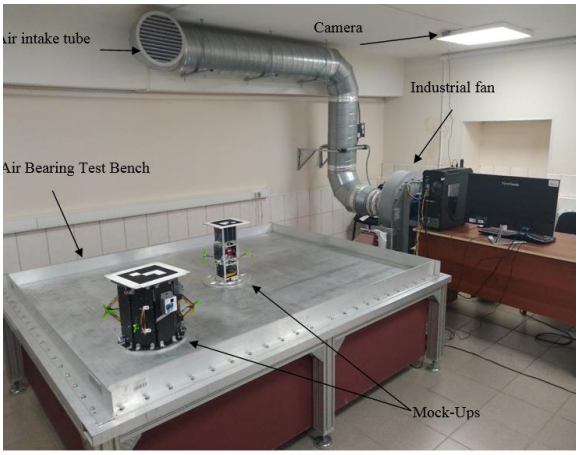

Fig. 13. Test facility COSMOS at the Keldysh Institute of Applied Mathematics

6. Controlled motion for debris observation

Consider the space debris and active satellite on the near circular orbits. For a long observation it is reasonable to choose a natural closed relative orbit. Such an orbit can be obtained using Clohessy-Wiltshire equations which has the following form:

$$\begin{aligned} \ddot{x} &= -2\dot{z}\omega, \\ \ddot{y} &= -y\omega^2, \\ \ddot{z} &= 2\dot{x}\omega + 3z\omega^2 \end{aligned} \qquad (19)$$

where $\mathbf{r} = \mathbf{r}_2 - \mathbf{r}_1 = (x, y, z)$ is the relative state vector in the orbital reference frame moving in the circular orbit with orbital angular velocity ω. The solution of (19) is

$$x(t) = -3C_1\omega t + 2C_2\cos\omega t - 2C_3\sin\omega t + C_4,$$
$$y(t) = C_5\sin\omega t + C_6\cos\omega t, \quad (20)$$
$$z(t) = 2C_1 + C_2\sin\omega t + C_3\cos\omega t$$

where the constants $C_1, C_2, C_3, C_4, C_5, C_6$ are defined by the initial conditions. In the common case the trajectory is elliptical spiral. The term responsible for the relative drift is $-3C_1\,\omega t$. The relative trajectory of two satellites is closed if and only if $C_1 = 0$. However, ideal initial conditions for a closed free motion cannot be achieved and it lead to slow change of instant ellipse position. To stop the drift the following Lyapunov-based control along the *x*-axis can be applied:

$$u_x = -kC_1,\ k > 0 \quad (21)$$

Consider the case when the active satellite observe the debris staying at the negative part of the *x*-axis. Assume that the observing sensors requires the maximal distance of $R_{\max}$. So, this value should not be achieved by the instant position of the ellipse in the case of zero drift is $C_4 - a$, where $a = \sqrt{C_2 + C_3}$ is the major semi axis of the ellipse and C_4 is instant position of the center of the ellipse along x-axis. Form the other hand in the observing stage the dangerous distance is also can be set as $R_{\min}$, where the collision with debris is possible. The closest distance can be calculated as $C_4 + a$. To avoid the collision the bang-bang control can be applied. For the impulsive thrust the algorithm can be described as follows:

$$u_x = \begin{cases} -2\omega C_1 / dt, \ if \ \ |C_4 + a| < R_{\min} \\ -\omega C_1 / dt, \ if \ \ |C_4 - a| > R_{safe} \end{cases} \quad (22)$$

When the dangerous distance is reached, the control changes the sign of the relative drift constant C_1 and the relative distance is increasing. When the distance reaches a safe distance R_{safe} that is less than $R_{\max}$ the drift is stopped by the second impulse. The similar approach can be applied if the satellite distance is approaches the maximal value $R_{\max}$ that is not suitable for the debris observation.

Such a control scheme is quite simple but it is reliable and robust. The most crucial problem in the observing stage if the relative motion determination. Assume that the active satellite equipped with laser range finder and the optical sensor for the pointing. The measurements of the laser range finder provide the distance to the debris and the optical sensors measures the unit vector direction angles in the orbital reference frame. This measurements are processed by the Kalman filter algorithm which estimate the 6-th dimensional state vector – relative position vector and relative velocity. Using this estimations the semi axis a and relative shift C_4 can be calculated. Since the optical sensors cannor measure in the shadow part of the orbit the current state vector is obtained by the integration of the motion equations using last obtained state vector. Since it is calculated with errors the covariance matrix can be used to calculate the error ellipse of the current and expected state vector.

Such a scheme of the motion of the active satellite for debris observation is implemented numerically. Fig 14 shows the relative trajectory of the active satellite, debris, dangerous distance and error ellipsoid. The relative position errors can be seen from Fig 15. The increase of the error is caused by absence of the measurements in the shadow part of the orbit. The relative distance is demonstrated at Fig 16. Initially the relative drift result in decreasing the distance but at the dangerous distance the impulse was applied and the satellite started drifting with another sign. When the safe distance was achieved the second impulse stopped the drift and the ellipse become almost closed.

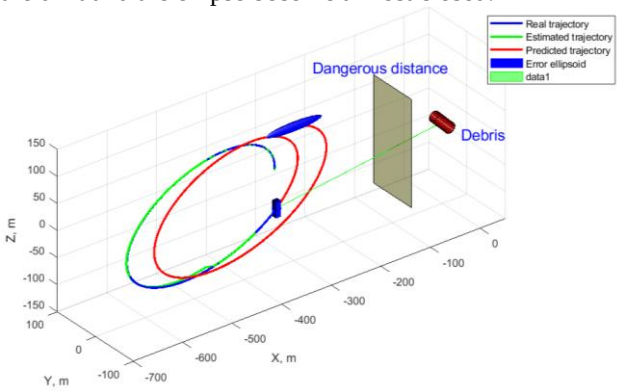

Fig. 14. Relative trajectory of the active satellite at the debris observation stage

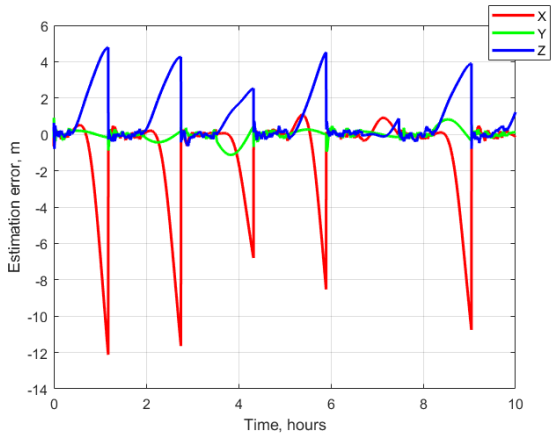

Fig. 15. Relative position estimation errors

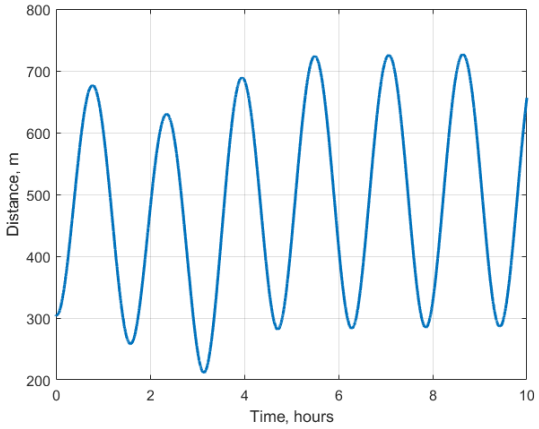

Fig. 16. Relative distance

The proposed scheme was tested using laboratory facility. One of the mock-ups is fixed on the table, the other is imitating active satellite. The orbital free motion is considered only in the orbital plane since the out-of-plane motion is always bounded that is suitable for the observation. The free orbital motion trajectory is calculated according to the orbital initial conditions and tracked by the on-board control system. Fig 17 shows the relative trajectory of the active mock-up relative to the debris mock-up. Initially trajectory has a drift towards the debris mock-up. At the dangerous distance of 0.4 m the collision avoidance manoeuvre was applied that changed the drift sign and the distance increased after two revolutions. After reaching the safe distance of 1m the drift was stopped by the second impulse as one can see on Fig 18. During the relative motion the laser range-finder imitator was pointed towards the debris. Fig 19 shows the required pointing angle and implemented by the control system. Its difference does not exceed 3-4 deg.

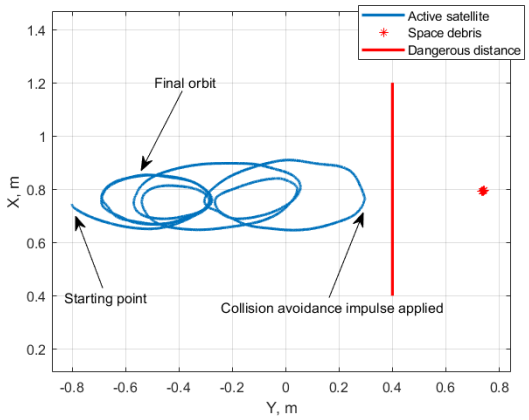

Fig 17. Trajectory of nanosatellite mock-up on air table

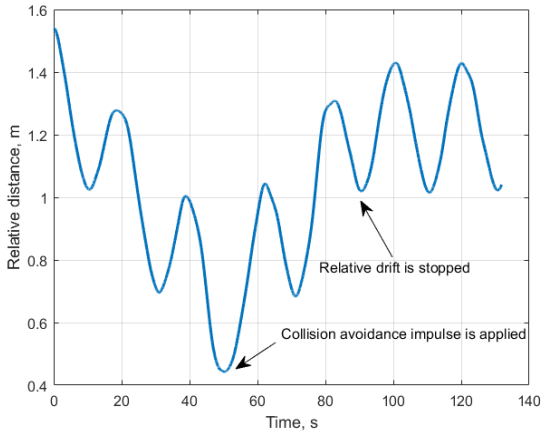

Fig. 18. Relative distance

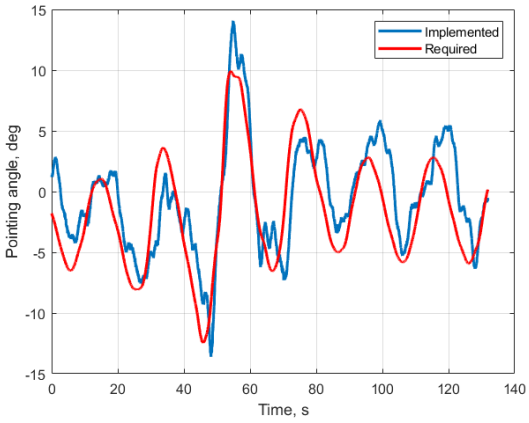

Fig. 19. Pointing angle: required and implemented

Thus, the simple relative motion control for debris observation is proposed and successfully tested on the air-bearing table. The orbital motion is imitated on the table only partly and the achieved accuracies will be not the same for the intended mission, nevertheless it demonstrates the controlled motion scheme implemented in hardware.

6. CONCLUSIONS

The proposed algorithms for controlled motion for space debris observation and for capturing using artificial potentials are successfully tested using laboratory facility on the air-bearing test-bed. The scheme of the collision avoidance at the stage of debris observation is simple and easy for implementation. The most critical part for implementation of this relative motion scheme is relative state vector estimation. The proposed algorithm based on extended Kalman filter provides an estimation using laser range finder measurements. Its errors are taken into account in relative distance calculation.

Acknowledgements

The work is supported by the Russian Foundation of Basic Research, grants № 20-31-90072, 18-31-20014

References

[1] Baranov A.A., Development of methods for calculating the parameters of spacecraft maneuvers in the vicinity of a circular orbit, keldysh institute of applied mathematics, 2019.

[2] J.A. Kechichian, Optimal low-thrust rendezvous using equinoctial orbit elements, Acta Astronautica. 38 (1996) 1–14. doi:10.1016/0094-5765(95)00121-2.

[3] T. Çimen, Survey of State-Dependent Riccati Equation in Nonlinear Optimal Feedback Control Synthesis, Journal of Guidance, Control, and Dynamics. 35 (2012) 1025–1047. doi:10.2514/1.55821.

[4] M. Akhloumadi, D. Ivanov, Satellite relative motion SDRE-based control for capturing a noncooperative tumbling object, in: Proceedings of 9th International Conference on Recent Advances in Space Technologies, RAST 2019, Institute of Electrical and Electronics Engineers Inc., 2019: pp. 253–260. doi:10.1109/RAST.2019.8767449.

[5] M. Navabi, M.R. Akhloumadi, Nonlinear Optimal Control of Relative Rotational and Translational Motion of Spacecraft Rendezvous, Journal of Aerospace Engineering. 30 (2017) 04017038. doi:10.1061/(ASCE)AS.1943-5525.0000749.

[6] A. Ruggiero, P. Pergola, S. Marcuccio, M. Andrenucci, Low-Thrust Maneuvers for the Efficient Correction of Orbital Elements, 32nd International Electric Propulsion Conference. (2011) 1–13.

[7] R. Falck, L. Gefert, A method of efficient inclination changes for low-thrust spacecraft, in: AIAA/AAS Astrodynamics Specialist Conference and Exhibit, American Institute of Aeronautics and Astronautics Inc., 2002. doi:10.2514/6.2002-4895.

[8] S. Geffroy, R. Epenoy, Optimal low-thrust transfers with constraints - Generalization of averaging techniques, Acta Astronautica. 41 (1997) 133–149. doi:10.1016/S0094-5765(97)00208-7.

[9] D.E. Kirk, Optimal control theory; an introduction, Prentice-Hall, 1970.

[10] M. Guelman, M. Aleshin, Optimal bounded low-thrust rendezvous with fixed terminal-approach direction, Journal of Guidance, Control, and Dynamics. 24 (2001) 378–385. doi:10.2514/2.4722.

[11] K. Holmström, A.O. Göran, M.M. Edvall, User's Guide for TOMLAB 7, Tomlab Optimization Inc. (2010).

[12] A.B. Modelon, JModelica. org User Guide, verison 1.17, (n.d.).

[13] F. Magnusson, J. Åkesson, Dynamic Optimization in JModelica.org, Processes. 3 (2015) 471–496. doi:10.3390/pr3020471.

[14] J. Åkesson, K.E. Årzén, M. Gäfvert, T. Bergdahl, H. Tummescheit, Modeling and optimization with Optimica and JModelica.org-Languages and tools for solving large-scale dynamic optimization problems, Computers and Chemical Engineering. 34 (2010) 1737–1749. doi:10.1016/j.compchemeng.2009.11.011.

[15] P.E. Rutquist, M.M. Edvall, PROPT-Matlab Optimal Control Software-ONE OF A KIND, LIGHTNING FAST SOLUTIONS TO YOUR OPTIMAL CONTROL PROBLEMS!, 2010.

[16] D. Ivanov, M. Koptev, Y. Mashtakov, M. Ovchinnikov, N. Proshunin, S. Tkachev, A. Fedoseev, M. Shachkov, Determination of disturbances acting on small satellite mock-up on air bearing table, Acta Astronautica. 142 (2018) 265–276. doi:10.1016/j.actaastro.2017.11.010.

[17] D.S. Ivanov, M.D. Koptev, Y.V. Mashtakov, M.Y. Ovchinnikov, N.N. Proshunin, S.S. Tkachev, A.I. Fedoseev, M.O. Shachkov, Laboratory Facility For Microsatellite Mock-Ups Motion Simulation, Journal of Computer and Systems Sciences International. 57 (2018) 115–130.

[18] D. Ivanov, M. Koptev, M. Ovchinnikov, S. Tkachev, N. Proshunin, M. Shachkov, Flexible microsatellite mock-up docking with non-cooperative target on planar air bearing test bed, Acta Astronautica. 153 (2018) 357–366. doi:10.1016/j.actaastro.2018.01.054.

[19] SputniX - Orbicraft, (n.d.). http://sputnix.ru/ru/products/eduru/orbikraft-1-0 (accessed December 2, 2016).